Vol. 5(17) Oct. 2015, PP. 2443-2454

Contents list available at IJMEC

International Journal of Mechatronics, Electrical and Computer Technology (IJMEC)

Journal Homepage: www.aeuso.org

PISSN: 2411-6173 - EISSN: 2305-0543

Simultaneous Tuning of Multi-Band Power System Stabilizer and Various IPFC-based Damping Controllers: An Effective method for Mitigation of Low frequency Oscillations

Hossein Shayeghi, Abdollah Younesi, Yashar Hashemi

Electrical Engineering Department, University of Mohaghegh Ardabili

***Corresponding Author's E-mail:** hshayeghi@gmail.com*

Abstract

In this paper, coordinated tuning of three band power system stabilizer (PSS3B) with interline power flow controller (IPFC) in single machine infinite bus power system is proposed. From the dynamic model of the power system equipped with IPFC, linear Phillips-Heffron model is established. The damping controllers considering the various control signals of the IPFC designed based on linearized model. Optimal tuning of the controllers formulated as an optimization problem and solved using krill herd optimization algorithm. The eigenvalues analysis and response of the system to step change in mechanical torque used to demonstrate the effectiveness of the proposed method. Studies reveal that the most effective input signal of IPFC utilized for damping the low frequency oscillation coordinated with PSS3B is found to be the input signal m_2, providing robust performance under different operation conditions.

Keywords: *PSS3B, IPFC, Krill Herd*

1. Introduction

The phenomenon that is very important and a real concern in the power industry is the stability of electromechanical oscillation, i.e., the low frequency oscillations having an oscillation frequency in the range of 0.2 Hz to 2 Hz. These oscillations limit the maximum amount of power that can be transferred over the transmission lines and sometimes may have disastrous consequences to the interconnected power systems stability, leading to partial or total black-outs. Therefore, equipment and procedures to damp these oscillations are required for safe operation of power systems and allow existent transmission networks to be used better. The traditional approaches to damp the power system oscillation are by adding a power system stabilizer (PSS) in the excitation system of the generators [1]-[3]. In These years using of FACTS devices and PSS has extended to improve stability. Considering that the PSS is one of important equipment to damp the mechanical oscillation of generators. Although PSS can relieve the mechanical oscillation of generators however there are some unstable inter-area modes that we can not dispel them without using FACTS devices, so PSS and FACTS devices have been used to enhance the damping [4]-[6]. FACTS devices are playing an increasing and major role in the operation and control of competitive power systems. However, uncoordinated local control of FACTS devices and PSSs may cause instability interactions. To improve overall system performance, many researches were

Article History:

IJMEC DOI: 649123/10164

Received Date: Jun. 05, 2015

Accepted Date: Sep. 10, 2015

Available Online: Sep. 19, 2015

made on the coordination between PSSs and FACTS POD controllers [7]-[11]. Some of these methods are based on the complex nonlinear simulation [7], [8], while the others are based on the linearized power system model. Using bio-inspired optimization algorithms for many power system control applications shows that these algorithms have very effective performance and they can find near optimal solutions. So, in this paper a new bio-based swarm intelligence algorithm, called Krill Herd (KH) is proposed for optimal tuning of the PSS3B and IPFC POD controller gains to stabilize a synchronous machine connected to an infinite bus power system. The KH algorithm is based on the description of the herding of the krill agents in response to specific biological and environmental processes. The objective function of each krill individual is defined as its distances from food and highest density of the agent [12]. In this paper firstly power system under study linearized and Phillips-Heffron model of the power system equipped with IPFC established. Then by eigenvalues analysis less damped or unstable modes specified. In the second stage PSS3B designed in multiple operating points for power system under study and then by calculation of eigenvalues the improvement of the system stability is shown. Analysis of the eigenvalues show that there are some modes that PSS3B cannot damp them well. In the third stage, PSS3B coordinated with POD controller for all four input signals of the IPFC, m_1, δ_1, m_2, and δ_2 separately tuned. Then eigenvalues analysis shows that POD controller for input signal of m_2 for IPFC coordinated with PSS3B have the best performance in power system stability. Also, response of the system to step change in input mechanical torque proves the results of the eigenvalues analysis.

2. PSS3B Model

The model of three band power system stabilizer (PSS3B) shown in Figure 1 has dual inputs of electrical power deviation and rotor angular frequency deviation. The signals are used to derive an equivalent mechanical power signal. The time constants T_1 and T_2 represent the transducer time constants, and T_{w1} and T_{w2} represents the washout time constants [13].

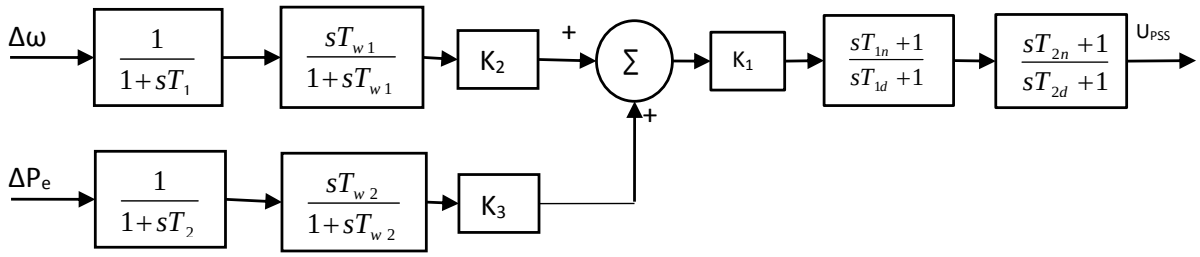

Figure 1: Structure of PSS3B

3. IPFC POD controller

The damping controller is designed to contribute a positive damping torque in phase with the speed deviation to the electromechanical oscillation loop of the generator. The structure of the IPFC based damping controller shown in Figure 2.

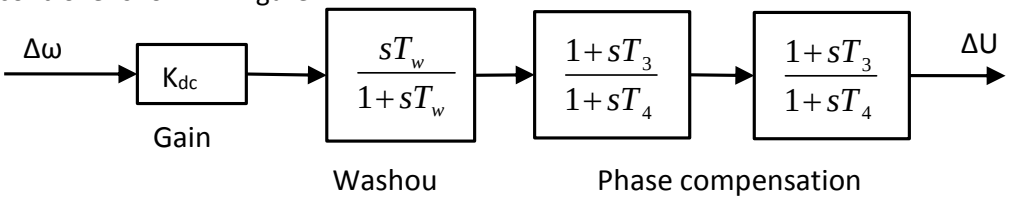

Figure 2: Structure of IPFC based POD controller

In the Figures 1 and 2 T_{w1}, T_{w2} and T_w are chosen 10. Also, for simplifying optimization problem value of T_{1n}, T_{2n}, T_{1d} and T_{2d} specified as 0.02, 0.03, 0.01 and 0.01 respectively. So, in optimization problem we have to find eight parameters T_1, T_2, K_1, K_2, K_3, K_{dc}, T_3 and T_4. Finding this parameters formulated as an optimization problem and solved using a new bio-inspired optimization algorithm called krill herd. In the next section a brief description of KH algorithm discussed. Equation (1) was used for fitness function of optimization.

$$fitness = \frac{(\sum_{i=1}^{N}[\int_{0}^{t_{sim}} t \mid \Delta\omega_i \mid dt]^2)}{N} \tag{1}$$

Where N is number of operation points, t_{sim} = 8 is simulation time.

4. Krill Herd Optimization Algorithm

Krill herd algorithm is one of the bio-inspired optimization algorithms that used for solving optimization problems. It inspired from the krill herding motions. This algorithm is based on the simulation of the herding of the krill swarms in response to specific biological and environmental processes. The time-dependent position on an individual krill in 2D surface is governed by the three main actions: movement induced by other krill individuals, foraging activity, and random diffusion. Equation (2) shows the lagrangian model of these three actions [13].

$$\frac{dX_i}{dt} = N_i + F_i + D_i \tag{2}$$

Where, N_i is the motion induced by other krill individuals, F_i is the foraging motion, and D_i is the physical diffusion of the ith krill individuals. Ni for a krill individual is calculated using Equation (3).

$$\begin{aligned} N_i^{new} &= N^{\max}\alpha_i + \omega_n N_i^{old} \\ \alpha_i &= \alpha_i^{local} + \alpha_i^{target} \end{aligned} \tag{3}$$

Where, N^{max} is the maximum induced speed, ω_n is the inertia weight of the motion induced in the range [0, 1], N_i^{old} is the last motion induced, α_i^{local} is the local effect provided by the neighbors, and α_i^{target} is the target direction effect provided by the best krill individuals. The foraging motion is formulated in term of two main effective parameters. The first one is the food location and the second one is the previous experience about food location. Equation (4) describes this motion.

$$\begin{aligned} F_i &= V_f \beta_i + \omega_f F_i^{old} \\ \beta_i &= \beta_i^{food} + \beta_i^{best} \end{aligned} \tag{4}$$

where, V_f is the foraging speed, ω_f is the inertia weight of the foraging motion in the range [0,1], F_i^{old} is the last foraging motion, β_i^{food} is the food attractive and β_i^{best} is the effect of the best fitness of the ith krill so far. The physical diffusion of the krill individuals is considered to be a random process, and is given by Equation (5).

$$D_i = D^{\max}\left(1-\frac{iter}{iter_{\max}}\right)\delta \tag{5}$$

Where, D^{max} is the maximum diffusion speed, and δ is a random directional vector and its arrays are random values between -1 and 1.

Finally, the position vector of a krill individual during the interval t to $t + \Delta t$ is given by Equation (6).

$$X_i(t+\Delta t) = X_i(t) + \Delta t \frac{dX_i}{dt} \tag{6}$$

Δt is a very important constant and should be carefully set according to the optimization problem. It completely depends on the search space and can be simply obtained using Equation (7).

$$\Delta t = C_t \sum_{j=1}^{NV}(UB_j - LB_j) \tag{7}$$

Where, NV is the total number of variables, LB_j and UB_j are lower and upper bounds of the jth variables, respectively, and C_t is a constant number between [0, 2]. Simplified flowchart of the krill herd algorithm is shown in Figure 3.

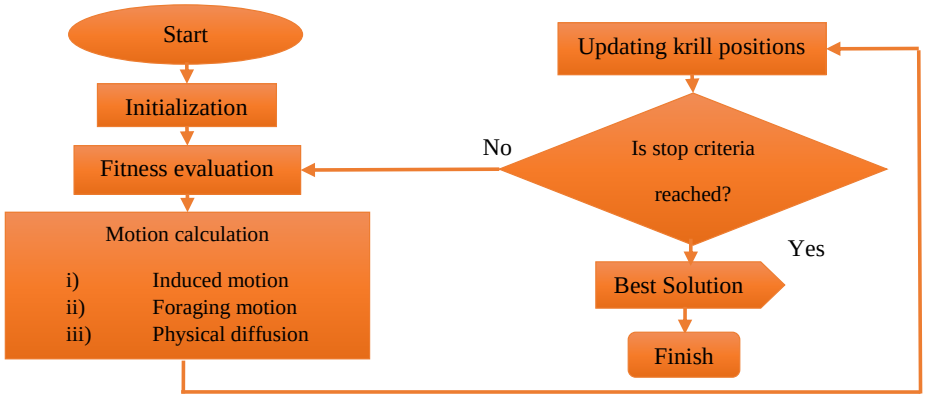

Figure 3: Flowchart of the KH algorithm

5. Dynamic Model of the SMIB Power System Equipped With IPFC

The power system under study shown in Figure 4. The system consists of a generator which is connected to the infinite bus through the two parallel transmission lines. An elementary IPFC consisting of two three phase GTO based VSCs, each compensating a different transmission line by series voltage injection is installed on the two transmission lines. The nonlinear dynamic model of the power system of Figure 4 described in Equations (8-12) as follows:

$$\dot{\delta} = \omega_0(\omega - 1) \tag{8}$$

$$\dot{\omega} = \frac{P_m - P_e - P_D}{2H} \tag{9}$$

$$\dot{E}_q' = \frac{(-E_q + E_{fd})}{T_{do}'} \tag{10}$$

$$\dot{E}_{fd} = \frac{-E_{fd} + K_a(V_{ref} - V_t)}{T_a} \tag{11}$$

$$\frac{dv_{dc}}{dt} = \frac{3m_1}{4C_{dc}}\begin{bmatrix}\cos\delta_1 & \sin\delta_1\end{bmatrix}\begin{bmatrix}i_{1d}\\ i_{1q}\end{bmatrix} + \frac{3m_2}{4C_{dc}}\begin{bmatrix}\cos\delta_2 & \sin\delta_2\end{bmatrix}\begin{bmatrix}i_{2d}\\ i_{2q}\end{bmatrix} \tag{12}$$

Where

$$P_e = P_1 + P_2 = v_{dt}i_{dt} + v_{qt}i_{qt} \quad , v_{qt} = E_q' - x_d' i_{dt} \quad , v_t = (v_{dt}^2 + v_{qt}^2)^{\frac{1}{2}} \quad , i_{dt} = i_{1d} + i_{2d}$$
$$E_q = E_q' + (x_d - x_d')i_{dt} \quad , v_{dt} = x_q i_{qt} \quad , i_t = i_{dt} + j i_{qt} \quad , i_{qt} = i_{1q} + i_{2q}$$

P_1, P_2 are the power flow in each of transmission lines and δ, is the rotor angle of the synchronous generator in radians, ω is rotor speed in rad/sec, V_t is the terminal voltage of the generator, E_q' is generator internal voltage, E_{fd} is the generator field voltage, v_{dc} is voltage at DC link. I_1 and I_2 are the transmission line currents. From Figure 4 we can get:

$$i_{1d} = x_{11d}E_q' + \frac{1}{2}(x_{12d} - x_{11d})v_{dc}m_2\sin\delta_2 - \frac{1}{2}x_{12d}v_{dc}m_1\sin\delta_1 - x_{11d}v_b\cos\delta \tag{13}$$

$$i_{2d} = x_{21d}E_q' + \frac{1}{2}(x_{22d} - x_{21d})v_{dc}m_2\sin\delta_2 - \frac{1}{2}x_{22d}v_{dc}m_1\sin\delta_1 - x_{21d}v_b\cos\delta \tag{14}$$

$$i_{1q} = \frac{1}{2}(x_{11q} + x_{12q})v_{dc}m_2\cos\delta_2 - \frac{1}{2}x_{12q}v_{dc}m_1\cos\delta_1 + x_{11q}v_b\sin\delta \tag{15}$$

$$i_{2q} = \frac{1}{2}(x_{21q} + x_{22q})v_{dc}m_2\cos\delta_2 - \frac{1}{2}x_{22q}v_{dc}m_1\cos\delta_1 + x_{21q}v_b\sin\delta \tag{16}$$

Where x_{11d}, x_{12d}, x_{21d}, x_{22d}, x_{11q}, x_{12q}, x_{21q} and x_{22q} are calculated based on x_d, x_d', x_{t1} and x_{t2}.

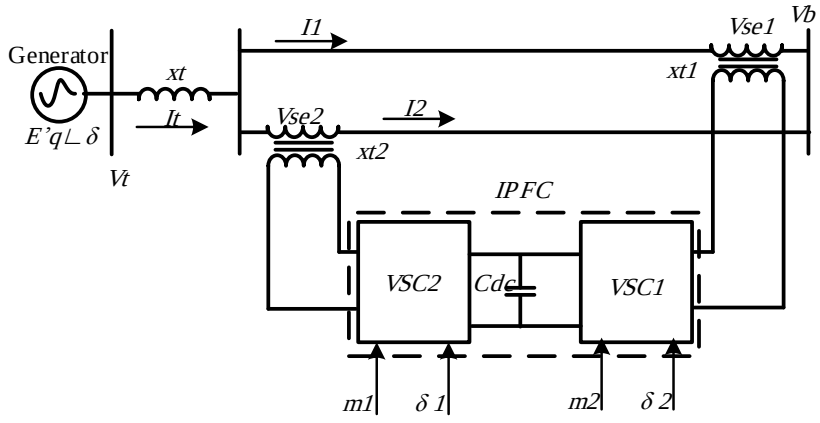

Figure 4: SMIB equipped with IPFC

6. Linearized Model

The linear Heffron-Philips model of SMIB system installed with IPFC is obtained by linearizing Equations (8-12).

$$\Delta\dot{\delta} = \omega_0 \Delta\omega \tag{17}$$

$$\Delta\dot{\omega} = \frac{\Delta P_m - \Delta P_e - D\Delta\omega}{2H} \tag{18}$$

$$\Delta\dot{E}'_q = \frac{(-\Delta E_q + \Delta E_{fd})}{T'_{do}} \tag{19}$$

$$\Delta\dot{E}_{fd} = \frac{-\Delta E_{fd} + K_a(\Delta V_{ref} - \Delta V_t)}{T_a} \tag{20}$$

$$\Delta\dot{v}_{dc} = K_7\Delta\delta + K_8\Delta E'_q - K_9\Delta v_{dc} + K_{cm1}\Delta m_1 + K_{c\delta 1}\Delta\delta_1 + K_{cm2}\Delta m_2 + K_{c\delta 2}\Delta\delta_2 \tag{21}$$

Where

$$\Delta P_e = K_1\Delta\delta + K_2\Delta E'_q - K_{pv}\Delta v_{dc} + K_{pm1}\Delta m_1 + K_{p\delta 1}\Delta\delta_1 + K_{pm2}\Delta m_2 + K_{p\delta 2}\Delta\delta_2 \tag{22}$$

$$\Delta E_q = K_4\Delta\delta + K_3\Delta E'_q - K_{qv}\Delta v_{dc} + K_{qm1}\Delta m_1 + K_{q\delta 1}\Delta\delta_1 + K_{qm2}\Delta m_2 + K_{q\delta 2}\Delta\delta_2 \tag{23}$$

$$\Delta V_t = K_5\Delta\delta + K_6\Delta E'_q - K_{vv}\Delta v_{dc} + K_{vm1}\Delta m_1 + K_{v\delta 1}\Delta\delta_1 + K_{vm2}\Delta m_2 + K_{v\delta 2}\Delta\delta_2 \tag{24}$$

The model has 28 K-constants which are functions of system parameters and the initial operating conditions [14].

7. Simulation Results

A single machine infinite bus power system installed with IPFC considered for analysis, parameters of which are given in [14]. In multiple operation points, Using KH algorithm optimization problem solved and parameters of the PSS3B and IPFC based POD controller obtained as Table 1.

Table 1: Optimization Results Using KH Algorithm

	K_1	K_2	K_3	K_{dc}	T_1	T_2	T_3	T_4
m_1 based POD controller	7.1116	2.8962	4.6266	4.0332	1.5952	1.1796	1.5607	0.6286
δ_1 based POD controller	9.2945	21.0805	10.2110	10.2559	1.6015	1.1180	0.8595	0.9755
m_2 based POD controller	15.4613	15.9442	1.2472	19.6475	0.3001	0.7086	0.6534	0.2601
δ_2 based POD controller	8.4403	13.4196	5.2152	7.0487	1.1988	1.6103	1.4488	0.9877
No POD controller (only PSS3B)	8.0120	11.2015	4.5261	-	1.0012	1.2350	-	-

Case1. No POD controller and No PSS3B

In this case of simulation, power system under study linearized around operating point *Pe* = 0.8 p.u. eigenvalues for the power system at this operating point are shown in Table 2. The system contains a pair of complex eigenvalues having low damping ratio 0.0086. In the following cases performance of various control methods on damping all oscillations is evaluated.

Table 2: Eigenvalues of the linearized SMIB at operating point *Pe* = 0.8 pu, without PSS3B and POD

Eigenvalues	Damping Ratio	Frequency
-98.4073	1	0
-0.0513±j5.9425	**0.008625221640320**	**5.9427**
-2.3173	1	0
-0.0011	1	0

Case2. Only PSS3B

The system eigenvalues in the presence of the PSS3B power system stabilizer is shown in Table 3. As shown in Table 3 the minimum complex eigenvalue pair's damping ratio has increased to approximately 0.1593. Response of the system to step change in mechanical torque shown in Figure 5.

Table 3: Eigenvalues of the linearized SMIB at operating point *Pe* = 0.8 pu, with PSS3B only

Eigenvalues	Damping Ratio	Frequency
-124.43	1	0
-86.37±j17.42	**0.980256973211417**	**88.1141**
-1.54±j9.54	**0.159345635145422**	**9.6678**
-0.72±j0.49	**0.826063434410464**	**0.8700**
-0.6020	1	0
-0.1040	1	0
-0.00115	1	0

Case3. PSS3B and POD controller m_1

The system eigenvalues in the presence of coordinated tuned PSS3B and m_1 based POD controller is shown in Table 4. As shown in Table 4 the minimum complex eigenvalue pair's damping ratio has increased to approximately 0.1797. Response of the system to step change in mechanical torque shown in Figure 6.

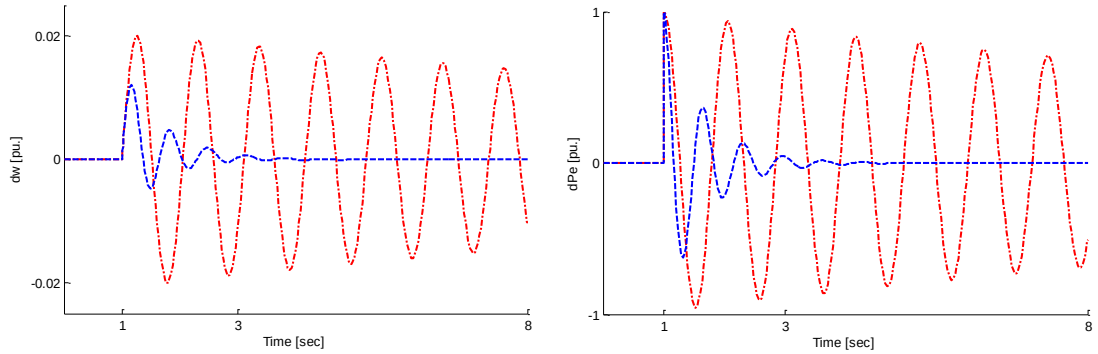

(a) **(b)**

Figure 5: Response of the system to step change in mechanical torque in operating point *Pe*=0.8 pu. With PSS3B only. (a): Rotor speed deviation, (b): Electrical power deviation. Red-dotted: No PSS3B and No POD, Blue-dashed: PSS3B and No POD.

Table 4: Eigenvalues of the linearized SMIB at operating point *Pe* = 0.8 pu, with PSS3B and m_1 POD

Eigenvalues	Damping Ratio	Frequency
-124.45	1	0
-86.3498±j17.4501	**0.980185486187202**	**88.0953**
-1.7219±j9.4275	**0.179673259981046**	**9.5835**
-1.7352	1	0
-1.4865	1	0
-0.7189±j0.4892	**0.826750168671739**	**0.8696**
-0.6020	1	0
-0.0011	1	0
-0.1040	1	0

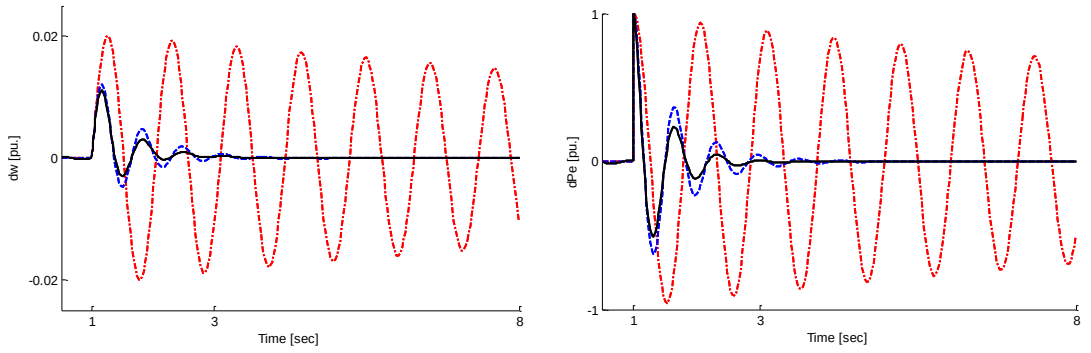

(a) **(b)**

Figure 6: Response of the system to step change in mechanical torque in operating point *Pe*=0.8 pu. With PSS3B and m_1 POD controller. (a): Rotor speed deviation, (b): Electrical power deviation. Red-dotted: No PSS3B and No POD, Blue-dashed: PSS3B and No POD, Black-solid: PSS3B and POD.

Case4. PSS3B and POD controller δ_1

The system eigenvalues in the presence of coordinated tuned PSS3B and δ_1 based POD controller is shown in Table 5. As shown in Table 5 the minimum complex eigenvalue pair's damping ratio has increased to approximately 0.2123 but the other mode's damping have decreased. Response of the system to step change in mechanical torque shown in Figure 7.

Table 5. Eigenvalues of the linearized SMIB at operating point *Pe* = 0.8 pu, with PSS3B and δ_1 POD

Eigenvalues	Damping Ratio	Frequency
-136.73	1	0
-78.9133±j23.6587	**0.957877291151762**	**82.3834**
-3.1862±j14.6622	**0.212349993300974**	**15.0044**
-0.5688±j0.3583	**0.846137863865611**	**0.6723**
-0.0011	1	0
-0.1255	1	0.8696
-0.3797	1	0
-1.0279	1	0
-1.0222	1	0

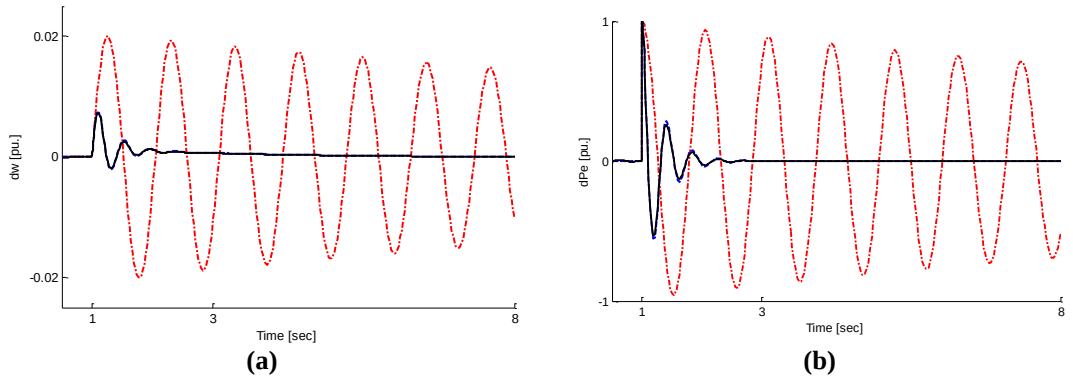

(a) **(b)**

Figure 7: Response of the system to step change in mechanical torque in operating point *Pe*=0.8 pu. With PSS3B and δ_1 POD controller. (a): Rotor speed deviation, (b): Electrical power deviation. Red-dotted: No PSS3B and No POD, Blue-dashed: PSS3B and No POD, Black-solid: PSS3B and POD.

Case5. PSS3B and POD controller m_2

The system eigenvalues in the presence of coordinated tuned PSS3B and m_2 based POD controller is shown in Table 6. As shown in Table 6 the minimum complex eigenvalue pair's damping ratio has increased to approximately 0.1327 and the other mode's damping ratio have increased well. Response of the system to step change in mechanical torque shown in Figure 8.

Table 6: Eigenvalues of the linearized SMIB at operating point *Pe* = 0.8 pu, with PSS3B and m_2 POD controller

Eigenvalues	Damping Ratio	Frequency
-124.1	1	0
-86.5187±j17.2178	**0.980767515535353**	**88.2153**
-1.2436±j9.2827	**0.132784514737628**	**9.3657**
-6.6311	1	0
-3.6551±j0.2794	**0.997091556188224**	**3.6657**
-0.7821±j0.2119	**0.965211482147324**	**0.8103**
-0.0011	1	0
-0.1129	1	0

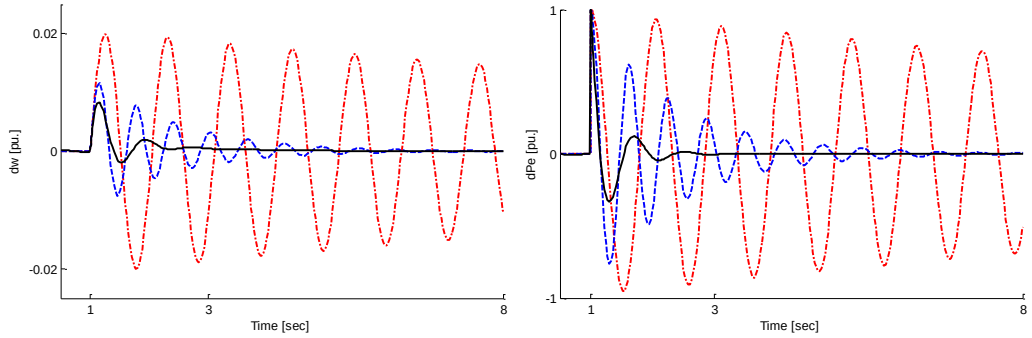

(a) **(b)**

Figure 8: Response of the system to step change in mechanical torque in operating point *Pe*=0.8 pu. With PSS3B and m_2 POD controller. (a): Rotor speed deviation, (b): Electrical power deviation. Red-dotted: No PSS3B and No POD, Blue-dashed: PSS3B and No POD, Black-solid: PSS3B and POD.

Case6. PSS3B and POD controller δ_2

The system eigenvalues in the presence of coordinated tuned PSS3B and δ_2 based POD controller is shown in Table 7. As shown in Table 7 the minimum complex eigenvalue pair's damping ratio has increased to approximately 0.1504. Response of the system to step change in mechanical torque shown in Figure 9. Based on simulation results δ_1 based POD controller is not suitable to be tuned coordinated with PSS3B. Whereas m_2 based POD controller prove to be suitable in order to tune coordinated with PSS3B to damp power system oscillations.

Table 7: Eigenvalues of the linearized SMIB at operating point *Pe* = 0.8 pu, with PSS3B and δ_2 POD controller

Eigenvalues	Damping Ratio	Frequency
-124.22	1	0
-86.4892±j17.2968	**0.980582901402733**	**88.2018**
-1.4418±j9.4714	**0.150489278085922**	**9.5805**
-1.3502	1	0
-0.0011	1	0
-0.1102	1	0
-0.5401±j0.1649	**0.956426114086947**	**0.5647**
-1.0077±j0.0249	**0.999694497177134**	**1.0080**

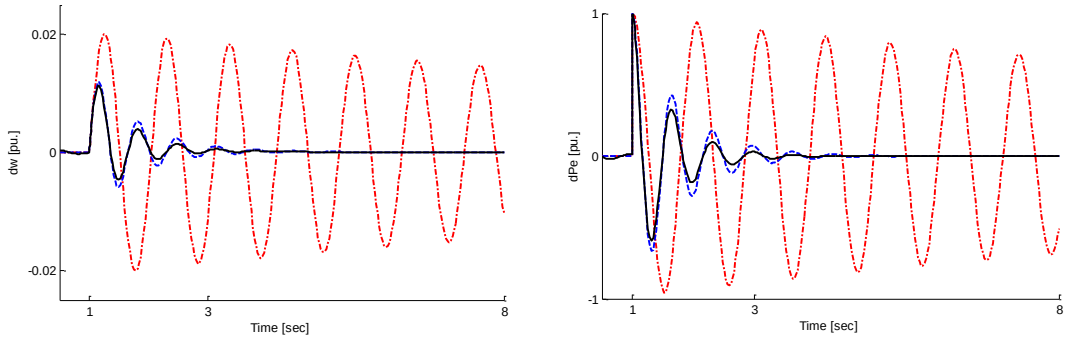

(a) **(b)**

Figure 9: Response of the system to step change in mechanical torque in operating point *Pe*=0.8 pu. With PSS3B and δ_2 POD controller. (a): Rotor speed deviation, (b): Electrical power deviation. Red-dotted: No PSS3B and No POD, Blue-dashed: PSS3B and No POD, Black-solid: PSS3B and POD.

Conclusion

In this paper, coordinated tuning of PSS3B with IPFC in single machine infinite bus power system is proposed. The damping controllers considering the various control signals of the IPFC designed based on linearized model. Optimal tuning of the controllers formulated as an optimization problem and solved using krill herd optimization algorithm. The eigenvalues analysis and response of the system to step change in mechanical torque used to demonstrate the effectiveness of the proposed method. Studies reveal that the most effective input signal of IPFC utilized for damping the low frequency oscillation coordinated with PSS3B is found to be the input signal m_2, providing robust performance under different operation conditions. Whereas the control signal δ_1 is inefficient in providing the damping coordinated with PSS3B.

References

[1] F. P. DeMello and C. Concordia, "Concepts of Synchronous Machine Stability as Affected by Excitation Control," *IEEE Transactions on Power Apparatus and Systems,* Vols. PSA-88, pp. 316-329, 1969.

[2] E. V. Larsen and D. A. Swarm, "Applying Power System Stabilizers, Parts I – III," *IEEE Transactions on Power Apparatus and Systems,* Vols. PSA-100, pp. 3017-3046, 1981.

[3] J. H. How and J. J. Sanchez-Gasca, "Pole Placment Design of Power System Stabilizers," *IEEE Transactions on Power Systems,* vol. 4, pp. 316-329, 1989.

[4] C. Li-Jun and I. Erlich, "Simultaneous Cooedinated Tuning of PSS and FACTS Damping Controllers in Large Power Systems," *IEEE Transactions on Power Systems,* vol. 20, no. 1, pp. 294-300, 2005.

[5] H. F. Wang, F. J. Swift and M. Li, "Comparison of Modal Controllability Between FACTS-based Stabilizers and PSS in Increasing the Oscillation Stability of Multimachine Power Systems," , (), pp. .," *IEE Proceedings Generation, Transmission and Distribution,* vol. 143, no. 6, pp. 575-581, 1996.

[6] Y. L. Abdel-Majid and M. A. Abido, "Optimal Multiobjective Design of Robust Power System Stabilizers Using Genetic Algorithms," 18 (3), pp.," *IEEE Transactions on Power Systems,* vol. 18, no. 3, pp. 1125-1132, 2003.

[7] C. Li-Jun and I. Erlich, "Fuzzy Coordination of FACTS Controllers for Damping Power System Oscillations," in *Int. Symp. Modern Electric Power Systems*, Wroclaw, Poland, 2002.

[8] X. Lei, E. N. Lerch and D. Povh, "Optimization and Coordination of Damping Controllers for Improving System Dynamic Performance," *IEEE Transactions on Power Systems,* vol. 16, no. 1, pp. 473-480, 2001.

[9] J. J. Sanchez-Gasca and J. H. Chow, "Power System Reduction to Simplify the Design of Damping Controllers for Inter-area Oscillations," *IEEE Transactions on Power Systems,* vol. 11, no. 3, pp. 1342-1349, 1996.

[10] P. Pourbeik and M. J. Gibbard, "Simultaneous Coordination of Power System Stabilizers and FACTS Devices Stabilizers in a Multimachine Power System for Enhancing Dynamic Performance," *IEEE Transactions on Power Systems,* vol. 13, no. 2, pp. 473-479, 1998.

[11] D. Arnautovic and J. Medanic, "Design of Decentralized Multi-Variable Excitation Controller in Multimachine Power Systems by Projective Controls," *IEEE Transactions on Energy Conversion,* Vols. EC-2, no. 4, pp. 598-604, 1978.

[12] A. H. Gandomi and A. H. Alavi, "Krill herd: A new bio-inspired optimization algorithm," *Communication in Nonlinear Science and Numerical Simulation,* vol. 17, no. 4, pp. 4831-4845, 2012.

[13] H. Shayeghi, A. Younesi, A. Akbarimajd and Y. Hashemi, "Robust Design of PSS3B Using KH Algorithm and Reinforcement Learning for Low-Frequency Oscillation Enhancement In SMIB Power System," in *6th Iranian Electrical and Electronic Engineering Conf*, Gonabad, Iran, 2014(in Persian).

[14] A. M. Parimi, Modeling and control of Interline Power Flow Controller for Power System Stability Enhancement, Perak: a Thesis submitted to the Postgraduate Studies Program in the University Teknologi Petronas, Malesia, 2011.